In-Situ Observation of Drying Process of a Latex Droplet by Synchrotron Small-Angle X-ray Scattering

Shanshan Hu,[†] Jens Rieger,[‡] Yuqing Lai,[†] Stephan V. Roth,[§] Rainer Gehrke,[§] and Yongfeng Men*[,†]

State Key Laboratory of Polymer Physics and Chemistry, Changchun Institute of Applied Chemistry, Chinese Academy of Sciences, Graduate School of Chinese Academy of Sciences, Renmin Street 5625, 130022 Changchun, P. R. China; BASF SE, Polymer Physics, 67056 Ludwigshafen, Germany; and HASYLAB am DESY, Notkestrasse 85, 22607 Hamburg, Germany

Received February 29, 2008
Revised Manuscript Received April 28, 2008

Introduction

Polymeric latex dispersions are widely used as paint, paper coating, and water-based adhesive. They are applied as liquid dispersions and form a film upon drying. It is generally accepted that there are three steps during the film formation process: evaporative drying and ordering, particle deformation, and polymer interdiffusion (for reviews see refs 1–3). Various aspects of the latex film formation process have been extensively studied by using analytical balance, atomic force microscopy (AFM), nonradiative energy transfer, etc.[4–14] Furthermore, scattering methods were proven to be useful to obtain insight into the structuring process on length scales from a few to some hundreds of nanometers in a nondestructive way.[15–30] Small-angle neutron scattering was used to study the film formation of latex dispersions, making use of enhanced contrast by adding D_2O.[19–23] Small-angle X-ray scattering (SAXS) has been used to investigate the crystallization process of charged colloidal dispersion.[24–28] Recently, the structure evolution in a latex film during stretching[29] and the appearance of macroscopically oriented colloidal crystals with fiber symmetry grown in a tube[30] were studied by means of synchrotron SAXS.

In this Note, the first two stages of film formation (i.e., water evaporation/particle ordering and particle deformation) was followed by using in-situ synchrotron SAXS. To reduce the influence of the substrate, the drying process of a latex droplet was followed by synchrotron SAXS measurements on a pending dispersion droplet of 2 mm diameter. All of the X-ray diffraction peaks can be easily indexed by assuming a face-centered-cubic (fcc) lattice structure. The structure evolution of the resultant crystallites was analysis of the change of the lattice constant.

Experimental Section

A styrene/*n*-butyl acrylate copolymer (T_g = 20 °C) with about 50 wt % of each monomer is used in this study. The average diameter of the spherical polymer latex particles was about 118 nm (see below). It is a commercially available raw material for coating and adhesion applications produced by BASF China. The system is stabilized against coagulation by negative surface charges on the latex particles originating from sulfate groups. The dispersion contains additional emulsifier and electrolyte. The density of the dried latex is 1.08 g/cm^3.

* Corresponding author. E-mail: men@ciac.jl.cn.
† Chinese Academy of Sciences.
‡ BASF SE.
§ HASYLAB am DESY.

Synchrotron SAXS measurements were performed at the beamline BW4 at HASYLAB, DESY, Hamburg, Germany. The energy of the X-ray radiation was 8.979 keV, resulting in a wavelength of 0.138 08 nm. The size of the primary X-ray beam at the sample position was 0.4 × 0.4 mm^2. The glass capillary (d = 1 mm) used in this investigation was mounted vertically onto a 2-dimensional translational stage. The latex dispersion with a solid content of ca. 40 wt % was injected into the glass capillary, yielding a droplet at the lower orifice. The sample-to-detector distance was 5694 mm. The effective scattering vector q ($q = (4\pi/\lambda)\sin\theta$, where 2θ is the scattering angle and λ the wavelength) range was 0.03−0.6 nm^{-1}. The dispersion was dried at 25 ± 1 °C and at a relative humidity of 30 ± 5%. SAXS patterns were collected with an exposure time of 30 s every 80 s with a 2D detector array (1024 × 1024 pixels, pixel size: 158.2 μm). The SAXS data were calibrated for background scattering and normalized with respect to the primary beam intensity.

Results and Discussion

Dispersion and Crystals. A photograph of a 40 wt % latex droplet at the bottom of the glass capillary is presented in Figure 1a. The contact area between the latex droplet and the glass tube is very small compared to the whole droplet; thus, the latex droplet measured in this experiment can be considered as an almost unconstrained sphere. Solidification proceeds for more than 2 h and is driven by water evaporation. The water evaporation rate was assumed to be identical anywhere on surface of the droplet. The resulting solid material is transparent to the naked eye with an air bubble in the center of the droplet. It is safe to assume that a skin of coalesced particles formed at the surface of the latex droplet initially with the water flux carrying latex particles from the inside toward the skin. As a result of this flux, an air bubble is formed in the center of the droplet. Figure 1b presents selected 2D SAXS patterns taken during the drying process. The drying time is indicated on each pattern. The observed intensity is the product of the structure factor $S(q)$ resulting from the crystalline ordering of the latex spheres and the single particle form factor $P(q)$ given by

$$I(q) \propto P(q)\, S(q) \tag{1}$$

The theoretical scattering intensity distribution of a sphere, i.e., the form factor $P(q)$, is given by[31]

$$P(q) \propto \frac{(\sin qR - qR\cos qR)^2}{(qR)^6} \tag{2}$$

where R is the radius of the sphere.

In order to describe the scattering intensity of dispersions, the hard-sphere model proposed by Percus and Yevick[32] was applied. It was shown by Ashcroft and Lekner[33] that this model leads directly to the structure factor of the dispersion, $S(q)$, and can be written in the following form[34]

$$S(q) = \frac{1}{1 - NpC(2qR)} \tag{3}$$

with

$$C(2qR) = -32\pi R^3 \int_0^1 \frac{\sin(2sqR)}{2sqR}(\alpha + \beta s + \gamma s^3)s^2\, \mathrm{d}s$$

where the volume fraction is defined by

$$\phi = \frac{4}{3}\pi R^3 N_p$$

The coefficients α, β, and γ are defined by

10.1021/ma800451n CCC: $40.75
Published on Web 06/04/2008

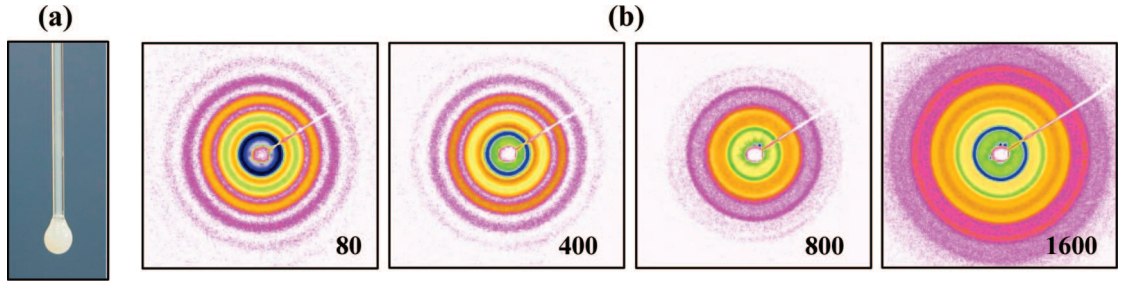

Figure 1. (a) Photograph of a 40 wt % latex droplet at the orifice of a glass tube. (b) Selected time-resolved SAXS patterns taken during the drying process of the latex droplet. The number indicated on each pattern denotes the drying time in seconds.

$$\alpha = (1+2\phi)^2/(1-\phi)^4$$
$$\beta = -6\phi(1+0.5\phi)^2/(1-\phi)^4$$
$$\gamma = 0.5\phi(1+2\phi)^2/(1-\phi)^4$$

To derive $P(q)$ directly and avoid the influence of $S(q)$, dilute latex dispersions were measured. This procedure is viable because $S(q)$ approaches close to unit in the experimental q range (0.03−0.6 nm^{-1}) for dispersions with a concentration of 1%. In this case, the system can be regarded as a suspension made of noninteracting particles. When polydispersity in particle size is also considered, the scattering intensity of the dilute system is[35]

$$I_0(q) = \sum_i N_i I_i^2(q) \quad (4)$$

where N_i denotes the number density of particles with size i.

Figure 2a presents the 1D SAXS intensity distribution of the latex at different concentrations. The discrepancy of scattering intensity data for the 1% latex dispersion at large q range is due to the limited exposure time and detector statistics. The data from the latex at higher concentrations show that the scattering curve differ in the small q range (<0.08 nm^{-1}); however, the shape of the curves at high q is hardly affected. All these data were fitted with the Percus−Yevick form assuming a radius of 59 nm of the latex particles (Figure 2a). It can be seen that the Percus−Yevick model describes the scattering behavior of the latex dispersions well. To obtain $P(q)$, scattering data from the 1% dispersion was fitted with eq 2. It was found that a form factor of a sphere with a radius of 59 nm fits the data best. When the polydispersity of the particle size distribution is considered, eq 4 must be applied to fit the data. Here a Gaussian distribution of the particle size distribution with a variance of 5% was used to fit the experimental data. It can be seen that the data can be described sufficiently well by assuming polydispersity. We also measured the size distribution using dynamic light scattering (DLS). The results show that the radius measured by DLS is about 10% larger than the radius determined by SAXS. This can be explained by the dragging of extra liquid along with the spheres.[36] The data at high volume fractions clearly show a correlation hole effect.

Figure 2b presents the integrated 1D SAXS intensity distribution of the latex after being dried for 133 min. Each Bragg peak is identified by assuming diffraction from an face-centered-cubic (fcc) crystal with the lattice constant of 143 nm (dashed lines). From this lattice constant, we calculated the size of the dried particles before deformation: $d = 2 \times d_{220} \times (100\%/74.1\%)^{1/3} = 111$ nm, where 74.1% is the volume fraction of close-packed spheres. This diameter is smaller than the size determined from the scattering of the dilute dispersion. This discrepancy may be due to again the dragging of extra liquid along with the spheres in dilute dispersion.[36] The occurrence of Debye−Scherrer

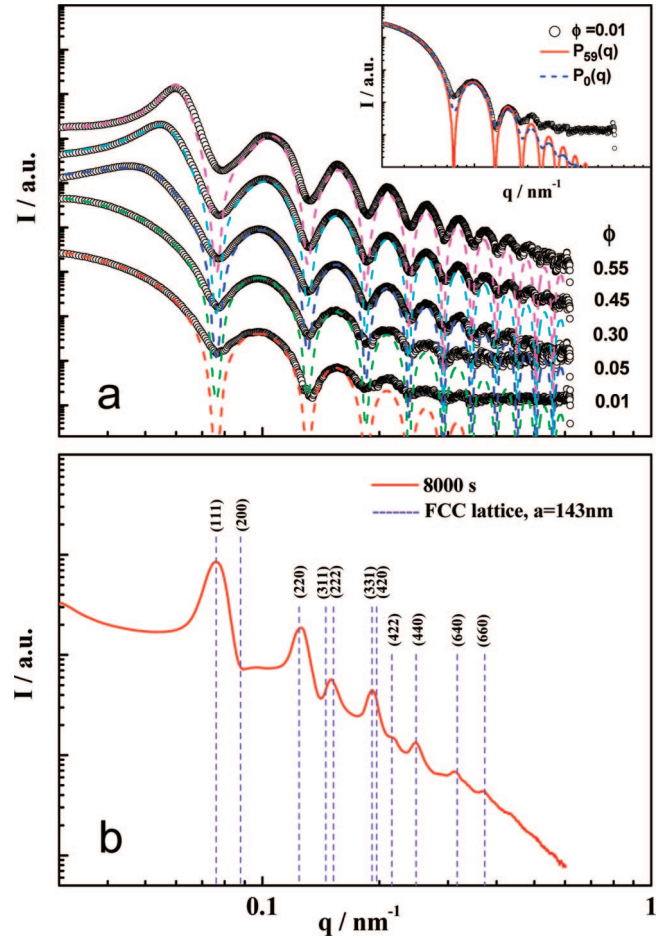

Figure 2. (a) Integrated 1D small-angle X-ray scattering intensity distribution of the latex dispersions at various concentrations (black open circles). The volume fraction ϕ of the latex dispersions is indicated on the plot. Each curve was fitted by using eqs 1–3 with a particle size of 59 nm (dashed line). Curves were vertically shifted for the sake of clarity. Inset: scattering data of a $\phi = 0.01$ dispersion (open circles); the form factor $P_{59}(q)$ calculated using eq 2 with a sphere radius of 59 nm (solid line) and the form factor $P_0(q)$ calculated using eqs 2 and 4 considering of a Gaussian distribution of particle size with the average radius of 59 nm and a variance of 5% (dashed line). (b) Integrated 1D SAXS intensity distribution of the latex after drying for 8000 s. The indices of an fcc crystalline structure with a lattice constant of 143 nm are indicated (dashed lines).

rings in Figure 1b implies that the polymeric spheres of the latex formed many randomly oriented crystallites resulting in a multidomain structure in the dried droplet.

From Figure 1b it is evident that a fraction of the primary X-ray beam was reflected at the interface of the latex and the bubble: the reflection was detected at small q value around the

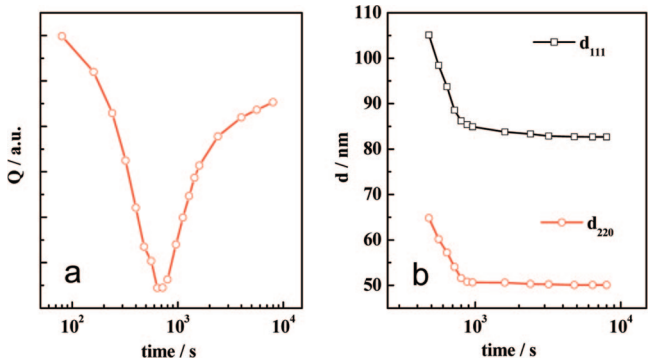

Figure 3. (a) Integral scattering intensity and (b) interplanar distance of (111) and (220) plane plotted as a function of drying time.

beam stop, seen as streaks in the last two patterns. From the analysis of integrated 1D SAXS intensity distribution, one observed a sharp increase of the scattering intensity at very small q value (0.03−0.05 nm^{-1}) after 560 s of drying, indicating the formation of the air bubble in the droplet.

Crystallization Process. The structural evolution of the latex droplet from the liquid to the crystalline state was followed by synchrotron SAXS. Since the final product consists of fcc crystallites and since the scattering peaks did not change qualitatively during drying (i.e., no lattice transition), it is safe to assume that the colloidal crystals with an fcc lattice structure formed during the evaporation of the water. The peak positions shifted to larger q values while the particles are approaching each other. The first two stages of film formation are water evaporation/particle ordering and particle deformation. Since a skin of coalesced particles was formed at the surface of the latex droplet initially, the particle ordering first occurred at the surface of the droplet. The center of the droplet initially remains liquid. Therefore, the initial data sets resulted from an overlapping of the scattering intensities from crystals and liquidlike structures. However, it is difficult to decompose the scattering data into contributions from these two phases. Fortunately, crystalline diffraction peaks are clearly identifiable from the data, and no further treatment of the data was needed. Before discussing the changes in the crystal lattice constant during drying, we look at the scattering power of the system. The scattering power Q is given by[37]

$$Q = V_{\mathrm{irr}}\Delta\rho_{\mathrm{e}}^{2}\phi(1-\phi) \propto \int_0^{\infty}\int_0^{\infty} I(q_x q_y)\,\mathrm{d}q_x\,\mathrm{d}q_y \qquad (5)$$

where V_{irr} is the volume of the sample irradiated by the X-rays, ϕ is the volume fraction of one phase, and $\Delta\rho_{\mathrm{e}}$ is the electron density difference between the phases in the system. The scattering power of the droplet decreases during the first 690 s and then increases (Figure 3a). The observed changes in scattering power can be discussed qualitatively using the above equation. During drying, V_{irr} becomes smaller while the product of $\phi(1-\phi)$ decrease when ϕ exceeds 50%. In addition, because the electron density of the liquid phase of water with salt and emulsifiers dissolved in the system is lower than that of latex particles, evaporation of water naturally leads to an increase of the electron density of the liquid phase, leading at first to a decrease of $\Delta\rho_{\mathrm{e}}$. Thus, at the beginning of the drying process the decrease in V_{irr} and $\Delta\rho_{\mathrm{e}}$ already outweighs the slight increase of the product of $\phi(1-\phi)$ before ϕ exceeds 50%. After the point where ϕ exceeds 50%, all factors lead to a decline of the Q value. However, the situation changes when ϕ reaches about 74% when particles start to contact. It should be mentioned that there is evidence that particle deformation can proceed before contact.[38–40] Beyond this point the intensity rises with further drying. This phenomenon might be explained using above argument on the change of $\Delta\rho_{\mathrm{e}}$ as follows: After water evaporation, the scattering results from the contrast between the particles and nonpolymeric material (salts, emulsifiers, etc.). This nonpolymeric material with a density higher than water is assumed to surround the particles homogeneously. Therefore, one expects a complete contrast matching at a certain concentration and an increase of $\Delta\rho_{\mathrm{e}}$ and thus Q thereafter until completely drying. At the point of contrast matching, a minimum Q value is observed as shown in Figure 3a. For ideal systems Q should be zero at this point because then $\Delta\rho_{\mathrm{e}} = 0$. This is not observed in our experiments and can be attributed to the nonhomogenous internal structure of latex particles which could also contribute to the scattering intensity.

The evolution of the interplanar distance shows that the shrinking rate was almost constant until the solid volume fraction reaches 91.4% (Figure 3b). Obviously, this rate was not affected by the particle deformation. The uniform rate of the evolution of the interplanar distance is in line with the observation that the latex dispersion always shows a constant drying rate.[2]

Conclusions

We have performed an in-situ synchrotron SAXS investigation on the drying process of a 40 wt % latex droplet. The first two stages of film formation, i.e., water evaporation/particle ordering and particle deformation, were recorded. Dilute suspensions were measured to determine the scattering single particle form factor and the particle size distribution. The resulting solid material was transparent to the naked eye with an air bubble in the center of the droplet. The SAXS pattern of the dried droplet revealed that colloid crystals with an fcc lattice were formed. It was found that the particle diameter determined by the scattering of a dilute dispersion is 10% smaller than the data from DLS but 7.5% larger than the diameter calculated from the dried fcc colloid crystal. The scattering intensity evolution has a turning point when the volume fraction of the particle reaches about 74%. The rate of the change of interplanar distances was almost a constant until the solid volume fraction is larger than 91.5%.

Acknowledgment. Y.M. thanks the Hundred Talents Project of the Chinese Academy of Sciences, National Natural Science Foundation of China (50621302), and HASYLAB project II-20052011.

References and Notes

(1) Keddie, J. L. *Mater. Sci. Eng. R* **1997**, *21*, 101–170.
(2) Winnik, M. A. *Curr. Opin. Colloid Interface Sci.* **1997**, *2*, 192–199.
(3) Steward, P. A.; Hearn, J.; Wilkinson, M. C. *Adv. Colloid Interface Sci.* **2000**, *86*, 195–267.
(4) Vanderhoff, J. W.; Bradford, E. B.; Carrington, W. K. *J. Polym. Sci., Polym. Symp.* **1973**, *41*, 155–174.
(5) Croll, S. G. *J. Coat. Technol.* **1986**, *58*, 41–49.
(6) Okubo, M.; Takeya, T.; Tsutsumi, Y.; Kadooka, T.; Umoto, T. M. *J. Polym. Sci., Polym. Chem. Ed.* **1981**, *19*, 1–8.
(7) Croll, S. G. *J. Coat. Technol.* **1987**, *59*, 81–92.
(8) Lin, F.; Meier, D. J. *Langmuir* **1995**, *11*, 2726–2733.
(9) Lin, F.; Meier, D. J. *Langmuir* **1996**, *12*, 2774–2780.
(10) Butt, H.-J.; Gerharz, B. *Langmuir* **1996**, *11*, 4735–4741.
(11) Farinha, J. P. S.; Martinho, J. M. G.; Yekta, A.; Winnik, M. A. *Macromolecules* **1995**, *28*, 6084–6088.
(12) Wang, Y.; Winnik, M. A. *J. Phys. Chem.* **1993**, *97*, 2507–2515.
(13) Pekcan, O.; Winnik, M. A.; Croucher, M. D. *Macromolecules* **1990**, *23*, 2673–2678.
(14) Wang, Y. C.; Kats, A.; Juhue, D.; Winnik, M. A. *Langmuir* **1992**, *8*, 1435–1442.
(15) Pusey, P. N.; van Megen, W.; Bartlett, P.; Ackerson, B. J.; Rarity, J. G.; Underwood, S. M. *Phys. Rev. Lett.* **1989**, *63*, 2753–2756.
(16) Pusey, P. N.; van Megen, W. *Nature (London)* **1986**, *320*, 340–342.

(17) Martelozzo, V. C.; Schofield, A. B.; Poon, W. C. K.; Pusey, P. N. *Phys. Rev. E* **2002**, *66*, 021408.
(18) Zhu, J. X.; Li, M.; Rogers, R.; Meyer, W.; Ottewill, R. H.; Russel, W. B.; Chailin, P. M. *Nature (London)* **1997**, *387*, 883–885.
(19) Joanicot, M.; Wong, K.; Maquet, J.; Chevalier, Y.; Pichot, C.; Graillat, C.; Lindner, P.; Rios, L.; Cabane, B. *Prog. Colloid Polym. Sci.* **1990**, *81*, 175–183.
(20) Chevalier, Y.; Pichot, C.; Graillat, C.; Joanicot, M.; Wong, K.; Maquet, J.; Lindner, P.; Cabane, B. *Colloid Polym. Sci.* **1992**, *270*, 806–821.
(21) Rieger, J.; Hadicke, E.; Ley, G.; Lindner, P. *Phys. Rev. Lett.* **1992**, *68*, 2782–2785.
(22) Joanicot, M.; Wong, K.; Cabane, B. *Macromolecules* **1996**, *29*, 4976–4984.
(23) Rieger, J.; Dippel, O.; Hadicke, E.; Ley, G.; Linder, P. In *Colloidal Polymer Particles*; Goodwin, J. W., Buscall, R., Eds.; Academic Press: London, 1995; pp 29−48.
(24) Sirota, E. B.; Ou-Yang, H. D.; Sinha, S. K.; Chaikin, P. M.; Axe, J. D.; Fujii, Y. *Phys. Rev. Lett.* **1989**, *62*, 1524–1527.
(25) Dingenouts, N.; Ballauff, M. *Langmuir* **1999**, *15*, 3283–3288.
(26) Dingenouts, N.; Ballauff, M. *Macromolecules* **1998**, *31*, 7423–7429.
(27) Dingenouts, N.; Ballauff, M. *Acta Polym.* **1998**, *49*, 178–183.
(28) Petukhov, A. V.; Aarts, D. G. A. L.; Dolbnya, I. P.; de Hoog, E. H. A.; Kassapidou, K.; Vroege, G. J.; Bras, W.; Lekkerkerker, H. N. W. *Phys. Rev. Lett.* **2002**, *88*, 208301.
(29) Men, Y. F.; Rieger, J.; Roth, S. V.; Gehrke, R.; Kong, X. M. *Langmuir* **2006**, *22*, 8285–8288.
(30) Hu, S. S.; Men, Y. F.; Roth, S. V.; Gehrke, R.; Reiger, J. *Langmuir* **2008**, *24*, 1617–1620.
(31) Roe, R.-J. *Methods of X-Ray and Neutron Scattering in Polymer Science*; Oxford University Press: New York, 2000; pp 155−162.
(32) Percus, J. K.; Yevick, G. J. *Phys. Rev.* **1958**, *110*, 1–13.
(33) Ashcroft, N. W.; Lekner, J. *Phys. Rev.* **1966**, *145*, 83–90.
(34) Ottewill, R. H. In *Colloidal Dispersions*; Goodwin, J. W., Ed.; The Royal Society of Chemistry: London, 1982; pp 197−217.
(35) Guinier, A. *X-Ray Diffraction In Crystals, Imperfect Crystals, and Amorphous Bodies*; Dover Publications: New York, 1994.
(36) Megens, M.; van Kats, C. M.; Boseche, P.; Vos, W. L. *Langmuir* **1997**, *13*, 6120–6129.
(37) Glatter, O.; Kratky, O. *Small-Angle X-ray Scattering*; Academic Press: London, 1982.
(38) Keddie, J. L.; Meredith, P.; Jones, R. A. L.; Donald, A. M. *Macromolecules* **1995**, *28*, 2673–2682.
(39) Crowley, T. L.; Sanderson, A. R.; Morrison, J. D.; Barry, M. D.; Morton-Jones, A. J.; Rennie, A. R. *Langmuir* **1992**, *8*, 2110–2123.
(40) Bonnet-Gonnet, C.; Belloni, L.; Cabane, B. *Langmuir* **1994**, *10*, 4012–4021.

MA800451N